




# Nickel phthalocyanine-borophene nanocomposite-based electrodes for non-enzymatic electrochemical detection of glucose

Gülşen Baytemir<sup>1,\*</sup> , İlke Gürol<sup>2</sup>, Selcan Karakuş<sup>3</sup>, Cihat Taştaltın<sup>2</sup>, and Nevin Taştaltın<sup>4,5,6,7,\*</sup>

<sup>1</sup>Department of Electrical and Electronics Engineering, Maltepe University, 34857 Istanbul, Turkey

<sup>2</sup>TUBITAK Marmara Research Center, Materials Institute, 41470 Kocaeli, Turkey

<sup>3</sup>Department of Chemistry, İstanbul University-Cerrahpaşa, 34320 Istanbul, Turkey

<sup>4</sup>Department of Basic Sciences, Maltepe University, 34857 Istanbul, Turkey

<sup>5</sup>Department of Renewable Energy Technologies and Management, Maltepe University, 34857 Istanbul, Turkey

<sup>6</sup>CONSENS Inc., Maltepe University Research Center, Technopark Istanbul, 34906 Istanbul, Turkey

<sup>7</sup>Environment and Energy Technologies Research Center, Maltepe University, 34857 Istanbul, Turkey

**Received:** 17 February 2022

**Accepted:** 8 June 2022

**Published online:**  
21 June 2022

© The Author(s), under exclusive licence to Springer Science+Business Media, LLC, part of Springer Nature 2022

## ABSTRACT

As diabetes has become one of the major health problems affecting hundreds of millions of people worldwide, the development of electrochemical sensors for the detection of glucose is crucial. Herein, the fabrication of nickel phthalocyanine (NiPc)-based and NiPc-borophene nanocomposite-based non-enzymatic electrochemical sensors for glucose detection at room temperature was demonstrated. The electrical conductivities of NiPc and NiPc-borophene nanocomposite have been measured as  $3 \times 10^{-13} \text{ S cm}^{-1}$  and  $9.5 \times 10^{-9} \text{ S cm}^{-1}$ , respectively. The electrical conductivity of NiPc has been improved with the addition of borophene. Due to the high charge transport advantages of the borophene additive, the sensor sensitivity and detection limit have been improved. In voltammetric cycle of 60 s for the 1.5–24 mM glucose concentration range, NiPc-based sensor has a sensitivity value of  $0.08 \mu\text{AmM}^{-1} \text{ cm}^{-2}$ , while the NiPc-borophene nanocomposite-based sensor has a much higher sensitivity of  $10.31 \mu\text{AmM}^{-1} \text{ cm}^{-2}$ . The limit of detection values of the NiPc and NiPc-borophene nanocomposite-based sensors are 3  $\mu\text{M}$  and 0.15  $\mu\text{M}$ , respectively. The borophene nanosheets with good chemical stability and high carrier mobility have been shown to be a good candidate to form nanocomposite structure with NiPc for glucose detection.

Address correspondence to E-mail: gulsenbaytemir@maltepe.edu.tr; nevintasaltin@maltepe.edu.tr

## 1 Introduction

Diabetes is a metabolic disorder in which pancreas produces insufficient or no insulin. Since the cells need insulin to absorb glucose to meet their energy needs, people with diabetes have an increase in glucose level in their blood while their cells suffer from glucose deficiency [1]. As diabetes has become the second major health problem affecting hundreds of millions of people worldwide, the development of biosensors for accurate and appropriate detection of glucose concentration is crucial [2–4]. In conventional glucose biosensors containing electrodes modified with enzymes such as glucose oxidase and glucose hydrogenase, the signal is obtained by the oxidation of hydrogen peroxide formed in the reaction of the enzymes. Although these electrodes have been significantly improved, the use of enzymes has some disadvantages arising from their stabilities and the sensitivities to temperature. Therefore, the development of non-enzymatic sensors has become of interest for research [2, 5–12].

Metal phthalocyanines (MPc) are thermally and chemically stable, highly delocalized systems with metal ions. Due to the fast redox chemistry, they have extended  $\pi$  systems that facilitate electron transfer for many molecules. Moreover, MPCs containing transition metals exhibit absorption in a very broad band range from the ultraviolet to the near infrared region [13]. Therefore, they are useful candidates for electrochemical applications such as electrocatalysis, supercapacitance. [14–17].

The studies in the literature have shown that nickel phthalocyanine (NiPc), Cobalt(II) phthalocyanine (CoPc), Copper(II) phthalocyanine (CuPc), Iron(II) phthalocyanine (FePc) and Zinc phthalocyanine (ZnPc) exhibit good electrocatalytic activities for the oxidation of common chemical substances such as hydrogen peroxide, nitrite, nitric oxide, cysteine and ascorbic acid [17–24]. In addition, there are some studies in which metalphthaloxyanin-based electrodes are used as redox mediators for glucose sensors [11]. However, due to the low electrical conductivity of MPCs, their properties are improved using them with conductive carbon materials or polymers for the applications on the electrode surfaces [16, 25, 26]. It has been reported that due to the strong  $\pi$  interaction between MPc and nanomaterials, they can be combined to form a stable composite structure. Since nanomaterials have a high surface

area-to-volume ratio, they provide high electrochemical activity. Therefore, with the increasing demand for improved device performance, special nanomaterials have begun to be fabricated. In the literature, there are several articles reported that metal phthalocyanines as sensing elements have redox interaction with glucose and graphene, carbon nanotubes, etc. Additions to metal phthalocyanines enhance the redox interactions in electrochemical sensor measurements [27–29]. Graphene with strong mechanical strength and high carrier mobility has been shown to be a good candidate to form composite with MPc [30, 31]. In 2015, the first theoretical studies of borophene as a two-dimensional nanomaterial like graphene were carried out [32–38]. In the light of these theoretical studies, it has been reported that borophene has chemical stability at room temperature. Borophene is a material with electrically semiconducting properties. As of 2018, there are only a limited number of articles in which borophene is prepared by wet-chemistry method. In these articles, the preparation of borophene in solution and its effect on the performance of the supercapacitors and the sensors were reported. It has also been reported that the electrical conductivity of the conductive polymer increases with the addition of borophene, as in the studies reporting that graphene as an additive material increases the conductivity of the conductive polymer [30, 31]. Borophene acts as an electrical conductivity-enhancing nanomaterial in the conductive polymer-borophene nanocomposite-based devices. It is predicted that the electrical conductivity of a metal phthalocyanine-borophene nanocomposite can be enhanced using the additive borophene, thereby improving the redox interaction between metal phthalocyanine-borophene nanocomposite and glucose in a non-enzymatic electrochemical sensor. However, there are no reports on the electrical conductivity and glucose interaction of NiPc-borophene nanocomposite as a non-enzymatic electrochemical sensor element.

From this point of view, in this study, NiPc-borophene nanocomposite-based non-enzymatic electrochemical sensor has been prepared, and the glucose sensing characteristics of the NiPc-borophene nanocomposite have been investigated in detail. The novelty of this work is the preparation, structural-chemical characterization, and glucose sensing mechanism of NiPc-borophene nanocomposite to be reported for the first time.

## 2 Experimental

### 2.1 Materials

For use in NiPc preparation, 1-Dodecanethiol ( $\geq 98\%$ ), Nickel (II) chloride hexahydrate ( $\text{NiCl}_2 \cdot 6\text{H}_2\text{O}$ ) (99%), quinoline (98%), potassium carbonate ( $\text{K}_2\text{CO}_3$ , 99%), anhydrous sodium sulfate ( $\text{Na}_2\text{SO}_4$ ,  $\geq 99$ ) were purchased from Sigma-Aldrich Company (Steinheim, Germany). Boron powder (95%) with an average particle size of 1.5  $\mu\text{m}$  used in the preparation of borophene nanosheet was purchased from Nanografi Company (Ankara, Turkey) and *N,N*-dimethylformamide (DMF) (ACS, 99.8 + %) from Merck Company (Darmstadt, Germany). All electrochemical measurements were taken using electrochemical gold transducers and Voltammetric Electrochemical Workstation purchased from Ebtron Electronics (Istanbul, Turkey).

### 2.2 Preparation of the borophene and nickel phthalocyanine-borophene nanocomposite

Borophene nanosheets were prepared by a simple and low-cost sonication method described in a previous work of our group [9]. 100 mg of boron powder (with a particle size of 1.5  $\mu\text{m}$ ) was sonicated in 100 mL of DMF under the nitrogen atmosphere at 200 W for 4 h. Next, in a two-step procedure, the solution was centrifuged for 15 min at 5000 rpm and 12,000 rpm, respectively. Finally, the collected borophene supernatant was dried in a vacuum oven for 12 h at 50  $^\circ\text{C}$  to obtain borophene. NiPc was synthesized according to reported procedures in [39]. Obtained borophene and NiPc materials were mixed 1:1 in chloroform and sonicated for 5 min. The preparation of NiPc-Borophene nanocomposite is schematized in Fig. 1.

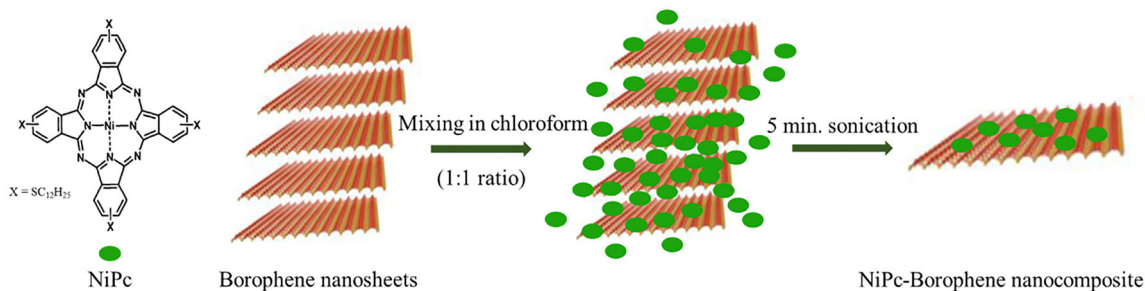


**Fig. 1** Schematic illustration of the preparation of NiPc-borophene nanocomposite

### 2.3 Preparation of NiPc-borophene-based non-enzymatic electrochemical biosensors and electrochemical measurements

Electrochemical measurements of the non-enzymatic glucose biosensor were performed with an Ebtron voltammetric electrochemical workstation. NiPc and NiPc-borophene nanocomposite-based electrodes were used as working electrodes. In general, for the electrochemical sensor fabrication, the electrodeposition method is used since it is convenient and efficient. However, the reproducibility of electrodeposition is limited for the preparation process and it is uncontrollable [40]. The modified electrode by drop-casting method overcomes the uncontrollability of electrodeposition process and the resultant glucose sensor would have repeatability, providing an efficient way for the fabrication of non-enzymatic glucose sensors. Therefore, after bare gold (Au) electrochemical transducers were cleaned with ethanol and dried, non-enzymatic electrochemical sensors were produced by coating NiPc and NiPc-Borophene nanocomposite on the transducers with a radius of 0.15 cm by drop-casting technique and drying at 40  $^\circ\text{C}$  (Fig. 2).

Then, in order to measure the detection of glucose at different concentrations with the produced biosensors, 1.5 mM, 3 mM, 6 mM, 12 mM and 24 mM glucose analytes were prepared using phosphate buffer solution (PBS). For all the electrochemical measurements, 3-electrode cyclic voltammetry method was used. Since this method is based on measuring the current response due to reduction or oxidation reaction in a solution, it was applied to determine the sensitivity of the prepared sensors. I–V characteristics of the biosensors for each glucose concentration were obtained by measuring the range

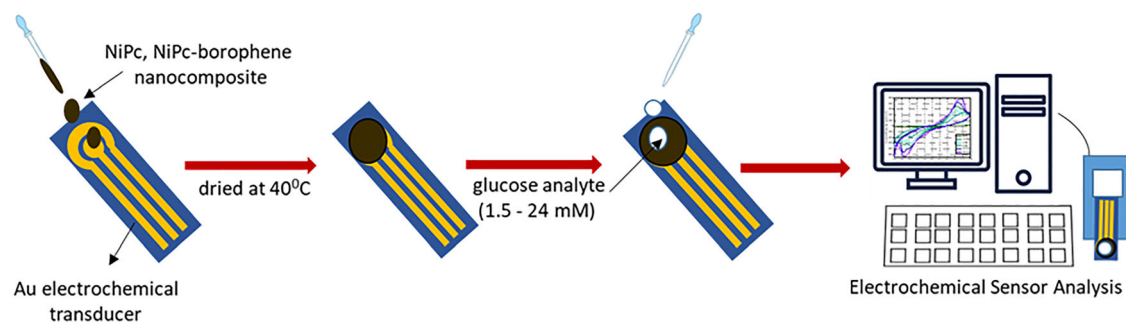


**Fig. 2** Schematic illustration of the non-enzymatic electrochemical sensor

of  $[-1, +1]$  V with a scanning rate of  $50 \text{ mV s}^{-1}$  in real-time measurements at  $25^\circ\text{C}$ .

## 2.4 Characterizations

The morphological and chemical properties of borophene and NiPc-Borophene nanocomposites were characterized by high-resolution transmission electron microscopy (HRTEM) (JEOL JEM-ARM200CFEG UHR-TEM), Scanning Electron Microscopy (SEM) (FEI QUANTA 450 model, conditions: a 6–10 mm working distance, 0–130 Pa pressure, and voltage of 7–10 kV under low vacuum medium), Fourier transform infrared spectroscopy (FTIR) (Perkin Elmer, Spectrum Two model, in the  $4000\text{--}400 \text{ cm}^{-1}$  frequency range with a resolution of  $4 \text{ cm}^{-1}$  and 8 scans), Raman spectroscopy (Renishaw in via Raman microscope, 2018 model), Laser ( $532 \text{ nm}$  ( $50 \text{ mW}$ ) and  $785 \text{ nm}$  ( $100 \text{ mW}$ )) and X-ray diffraction (XRD) with Cu  $K\alpha$  radiation at  $40 \text{ kV}$  and  $15 \text{ mA}$  using a Highscore Plus XRD program. Furthermore, SEM images of the prepared NiPc-Borophene nanocomposites were powered using an artificial intelligence (AI) approach.

## 3 Results and discussion

HRTEM and XRD analysis of the borophene are given in Fig. 3. According to HRTEM image given in Fig. 3a, it is understood that borophene obtained by sonication method in DMF medium exists in nanosheets and the nanosheets have crystalline structure with  $0.41 \text{ nm}$  stripe pitch, matching the characteristics of a  $\beta$ -rhombohedral boron structure [41]. An individual borophene nanosheet was also examined by Fast Fourier Transform (FFT) diffraction pattern given in the inset of Fig. 3a.

The crystallinity and the phase of the nanosheets were examined by XRD results. In Fig. 3b, we observed that XRD peaks correspond to (0001) plane of  $\beta$ -rhombohedral boron (PDF31-0207). The results of HRTEM and XRD analyzes are in agreement. Furthermore, the crystalline size of the synthesized nanostructure is calculated using Scherrer equation [42] (Eq. 1).

$$D_p = \frac{0.94 \cdot \lambda}{\beta \cdot \cos \theta} \quad (1)$$

where  $\lambda$  is the X-ray wavelength ( $0.15406 \text{ nm}$ ),  $\beta$  is full width at half maximum (FWHM),  $D$  is crystallite size diameter, and  $\theta$  is Bragg's diffraction angle obtained from 2-Theta values. According to the experimental results, the average crystalline size of borophene was calculated as about  $16.84 \text{ nm}$ .

As known, XRD of nanocomposite can not be detected as an intense peak due to its amorphous phase. However, it was seen as a broad peak due to scattering from a wide range of directions compared to lattice scattering in crystals in Fig. 3c.

In Fig. 4, SEM images of (a) NiPc ( $168.00\times$ ), (b) NiPc ( $42.000\times$ ), (c) NiPc-Borophene nanocomposites ( $1300\times$ ), (d) NiPc-Borophene nanocomposites ( $5700\times$ ), (e) NiPc-Borophene nanocomposites ( $5700\times$ ) aided by artificial intelligence, and (f) 3D imaging of the SEM image of NiPc-Borophene nanocomposite were presented. According to SEM images of NiPc, surface of NiPc was uniformly arranged with spherical shaped particles (Fig. 4a, b). As seen in Fig. 4c, d, it was determined that the nanostructure has spherical structures with particle sizes ranging from  $10$  to  $80 \text{ nm}$ , with the uniform morphology with the addition of the borophene [43]. SEM is one of the most preferred methods that provides understanding of the morphology of samples. However, sometimes it is not easy to observe high

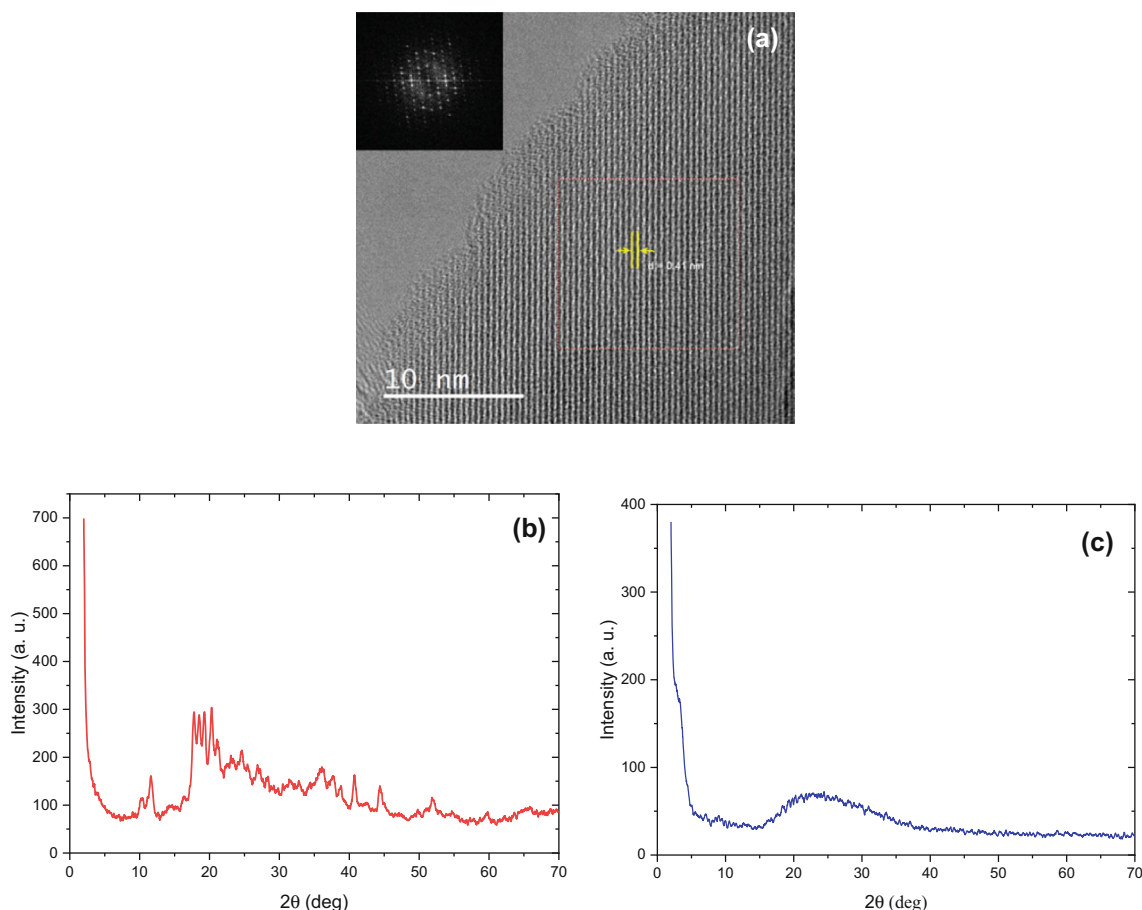


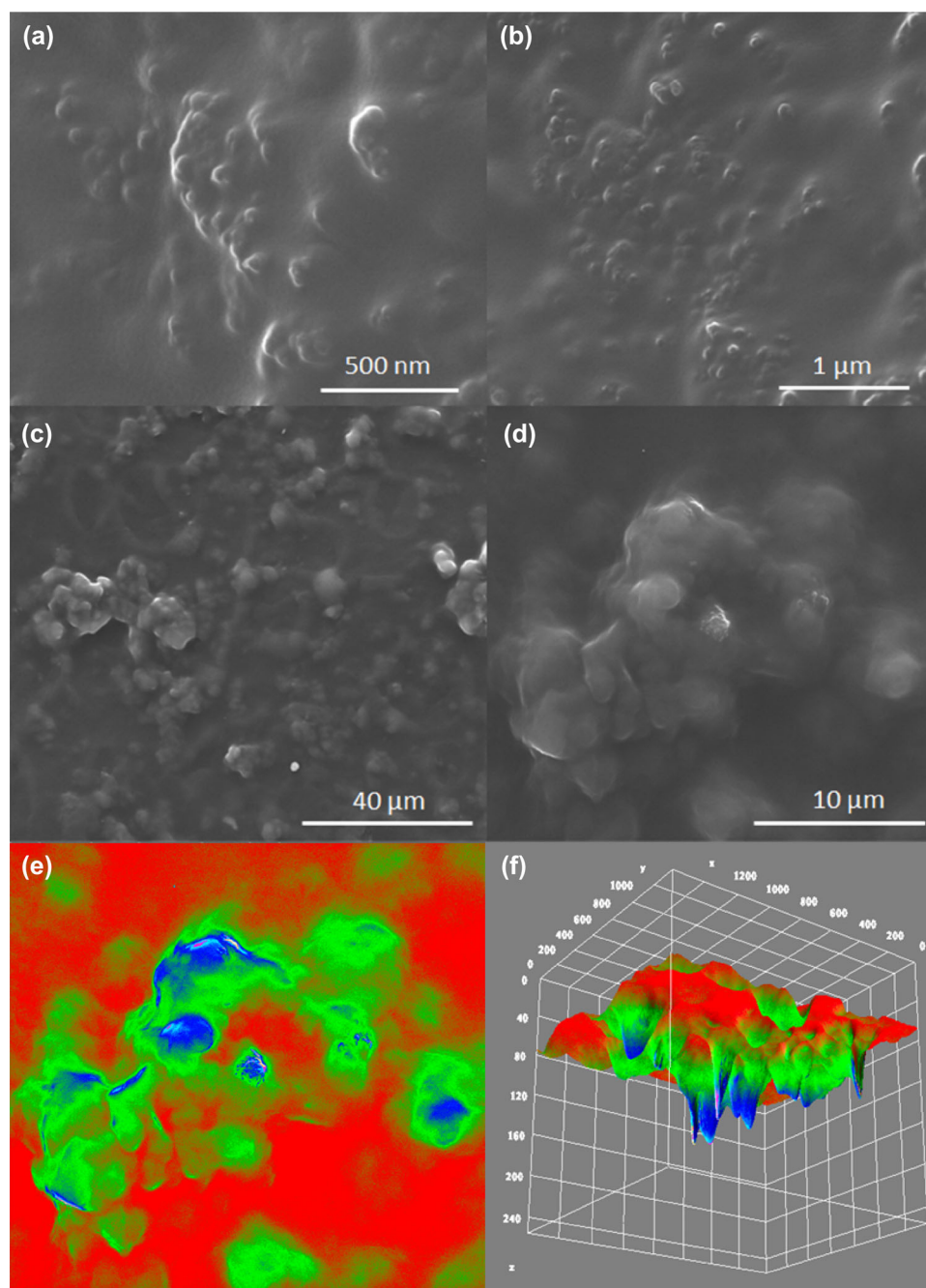
**Fig. 3** **a** HRTEM image of the freestanding borophene nanosheets, **b** XRD analysis of the borophene nanosheets, **c** XRD analysis of the NiPc-Borophene nanocomposite

quality SEM images due to operator skill and experimental process [44, 45]. To eliminate these experimental problems, we used an easy and low-cost AI-based method to enhance the quality of SEM images and to evaluate the coating efficiency of borophene in the matrix. The AI-powered SEM image of the NiPc-Borophene nanocomposite after image (8-bit) processing by ImageJ software and 3D surface plot of the AI-powered SEM image are presented in Fig. 4e, f. Here, a modified micrograph of the nanostructure is presented to extract the morphology of the NiPc-borophene nanocomposite using image algorithms convert them to 3D. It was understood that the distributions of nanostructure and their surface properties obtained with the unmodified SEM images in Fig. 4f. and those obtained using AI-powered SEM image were significantly different. The results showed a there is a relationship between the spherical shape of the particles and the matrix revealing a color pixel correlation between the two

phases. In Fig. 4e, the RGB values of the matrix were found as 233.18, 50.98, 34.93 for the polymer matrix and 20.46, 54.68, 225.54 for the red, green, and blue colors for the borophene additive, respectively. The AI-powered SEM image of the NiPc-borophene nanocomposite confirmed the interaction between the active surface functional groups of polymer matrix (red) and the borophene additive (green-blue). These differences of color pixels reflected the distribution of particles in the structure.

In Fig. 5, FTIR spectrum of the borophene, NiPc, and NiPc-borophene were given to observe functional groups of all samples. In our previous study, the characteristic peaks of the borophene were reported and according to these results, it was stated that the peaks were observed at  $3479\text{ cm}^{-1}$  (O–H),  $2929\text{ cm}^{-1}$  (B–B),  $2861\text{ cm}^{-1}$  (B–H),  $1653\text{ cm}^{-1}$  (C=O),  $1496\text{ cm}^{-1}$  (B–H),  $1385\text{ cm}^{-1}$  (B–O),  $1255\text{ cm}^{-1}$  (B–O), and  $1091\text{ cm}^{-1}$  (B–O–B vibrations) [9]. The peaks of the prepared NiPc were observed at  $3504\text{ cm}^{-1}$  (N–H

**Fig. 4** SEM images of **a** NiPc (168.00 $\times$ ), **b** NiPc (42.000 $\times$ ), **c** NiPc-borophene nanocomposite (1300 $\times$ ), **d** NiPc-borophene nanocomposite (5700 $\times$ ), **e** NiPc-borophene nanocomposite (5700 $\times$ ) aided by artificial intelligence, and **f** 3D imaging of SEM image of NiPc-borophene nanocomposite



stretching), 2920  $\text{cm}^{-1}$  (C–H) and 1680  $\text{cm}^{-1}$  (C=N/C=C). Additionally, the characteristic peaks of the prepared NiPc were at 1090  $\text{cm}^{-1}$ , 845  $\text{cm}^{-1}$ , and 756  $\text{cm}^{-1}$  attributed to the phthalocyanine skeletal vibrations [46]. The characteristic peaks of the prepared NiPc-borophene were found at 2922  $\text{cm}^{-1}$  (C–H), 1462  $\text{cm}^{-1}$  (–CN group), and 748  $\text{cm}^{-1}$  (bending modes of vibration of nickel) [47]. Consequently, the appearance of –CN group at 1462  $\text{cm}^{-1}$  and disappearance of the –NH peak at 3504  $\text{cm}^{-1}$  in the

structure confirmed the formation of the NiPc-borophene. The changes of intensity of the FTIR peaks of NiPc-borophene nanocomposite were indicative of the fact that borophene was dispersed into the NiPc matrix.

For the Raman spectral investigation of the NiPc sample on the glass and Raman scattering data, for NiPc and borophene shown in Fig. 6 confirmed the observations obtained from the FTIR spectra.

Moreover, Table 1 summarizes the assignments for the Raman bands.

The assignment of vibrations in the spectra of NiPc corresponds to  $\nu(\text{Ni-N})$  stretching vibrations on the

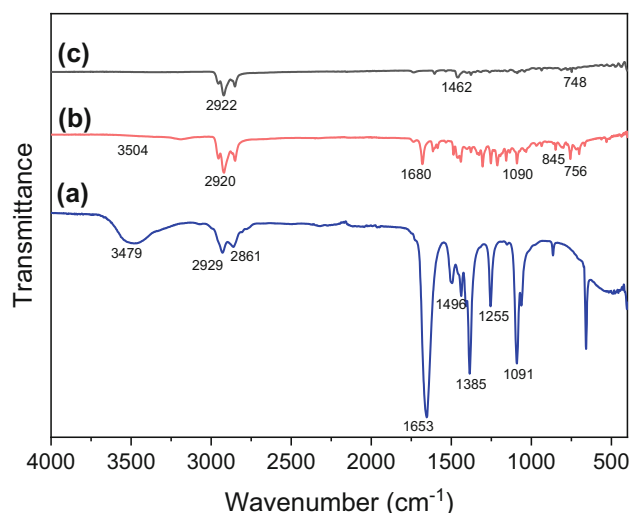


**Fig. 5** FTIR spectrum of (a) borophene, (b) NiPc, and (c) NiPc-borophene nanocomposite

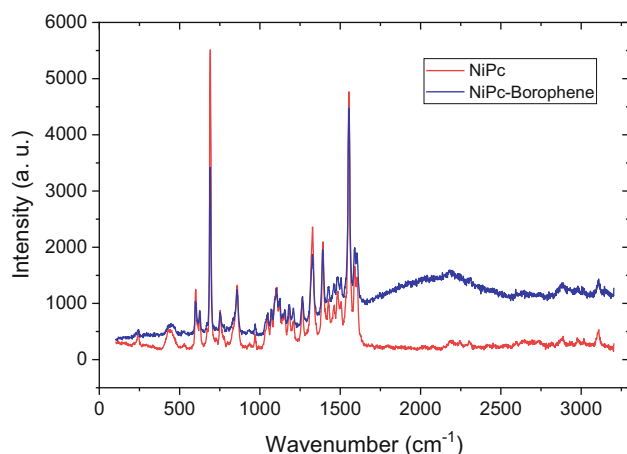


**Fig. 6** The Raman spectroscopy analysis of NiPc and NiPc-borophene nanocomposite

basis of comparison with Raman spectra of the band at  $245 \text{ cm}^{-1}$ . The main contribution to the vibration at  $1555 \text{ cm}^{-1}$  is given by displacements of the C–N–C bridge bonds of the phthalocyanine macrocycle [50]. The most intense bands can be seen in the range of  $1300\text{--}1600 \text{ cm}^{-1}$  and are generally due to the C–C pyrrole stretch in plane and C–N stretch. The bands at around  $690 \text{ cm}^{-1}$  which can be seen for all the samples occur due to the plane bending of carbon nitrogen bond. The bands between  $200$  and  $300 \text{ cm}^{-1}$  represent C–N–C in plane vibrations and the bands between  $800$  and  $1200 \text{ cm}^{-1}$  show either C–N, C–C stretches or C–H bending. Besides, when the NiPc and borophene mixed for the detection of glucose, various peaks belong to borophene were observed at  $1180$ ,  $1070$ ,  $751$  and  $447 \text{ cm}^{-1}$  in Raman [51].

Electrical conductivities of the NiPc and the NiPc-borophene nanocomposite were measured using four-probe station. Electrical conductivities of the NiPc and the NiPc-Borophene nanocomposite were

**Table 1** Assignment of Raman bands for NiPc and borophene

Assignment	NiPc	Borophene
Ni–N–; N–Ni–N	245	447 [48]
Macrocycle vibration	600	
Macrocycle vibration	691	751 [49]
Benzene breathing	969	
C–H bending	1049	
Inter-icosahedral B–B		1070
C–H bending	1104	1180 [48]
C–H bending	1263	
Pyrrole stretch	1327	
Isoindole stretch	1392	
Isoindole stretch	1484	
C=C, C=N pyrrole stretch	1555	
Benzene stretch	1603	

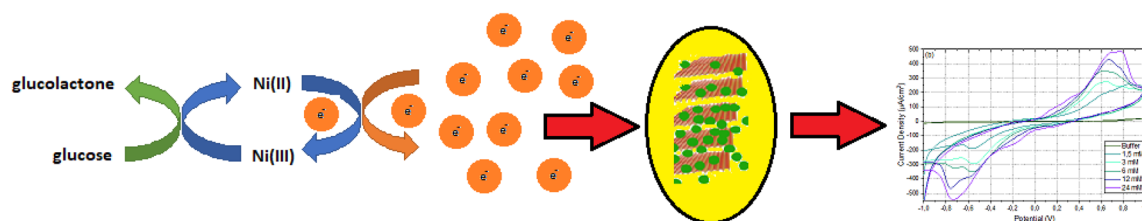


**Fig. 7** Schematic of glucose detection mechanism

found as  $3 \times 10^{-13} \text{ S cm}^{-1}$  and  $9.5 \times 10^{-9} \text{ S cm}^{-1}$ , respectively. This result reveals that borophene enhances the electrical conductivity of the NiPc approximately 10,000 times.

Borophene polymorphs share a triangular lattice with periodic hollow hexagones in the 2D limit. The material structure favors multicenter bonds, which makes most of borophene polymorphs metallic [37, 52–54] and this structure shows metallic properties. There could be such a possible reason. The change in the oxidation state of Ni(II) and Ni(III) could stem from of doing pile up on each other NiPc and borophene which play a role in the process of electrochemical oxidation cycle reaction. Firstly, Ni(II) of NiPc is oxidized to Ni(III) after that, Ni(III) could catalytically oxidize glucose to produce gluconolactone and is reduced to Ni(II). As the cycle continues, the electron produced in the oxidation of Ni(II) enters the electrochemical cycle through borophene, the electron acceptor, and generates the current response after glucose injected [55] (Fig. 7).

The sensors were tested for the glucose concentrations of 1.5, 3, 6, 12 and 24 mM. The sensitivity, response time and limit of detection (LOD) of the sensors were determined via electrochemical measurements of the sensor based on NiPc-borophene nanocomposite, in line with the electrocatalytic oxidation of glucose using the cyclic voltammetry method (Fig. 8). In the electrochemical step coupled to chemical oxidation on the surface of the NiPc-borophene nanocomposite, re-oxidation of the metal in NiPc was observed as anodic current due to the presence of glucose in the measuring cell. The nanocomposite of borophene with NiPc has improved the electrical conductivity of this sensor material (Fig. 8a, b).

The sensitivities of the NiPc and NiPc-borophene nanocomposite-based sensors were obtained by calculating the slope of current density versus glucose concentration curves shown in Fig. 8c. The graph depicts that while NiPc-based sensor has a sensitivity of  $0.08 \mu\text{AmM}^{-1} \text{ cm}^{-2}$ , the NiPc-borophene nanocomposite-based sensor has a much higher sensitivity,  $10.31 \mu\text{AmM}^{-1} \text{ cm}^{-2}$  during 1 min cyclic voltammetry measurement. The limit of detection values of the NiPc and NiPc-borophene nanocomposite-based sensors were calculated as  $3 \mu\text{M}$  and  $0.15 \mu\text{M}$ , respectively. The addition of borophene caused the detection limit of the NiPc-borophene composite-based sensor to have a much lower value. Table 2

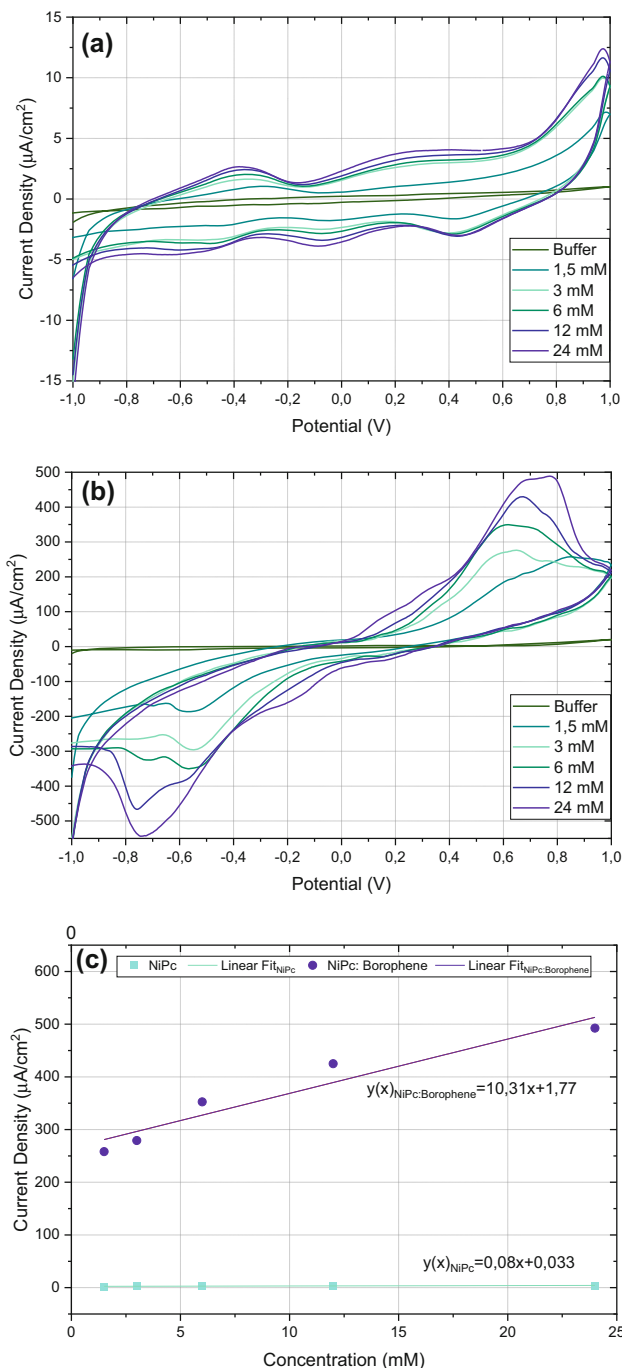


**Fig. 8** Sensor responses of **a** NiPc, **b** NiPc-borophene nanocomposite, **c** Comparative sensitivities of NiPc and NiPc-borophene nanocomposite for various concentrations of glucose

shows the electrochemical biosensors used for the detection of glucose and summarizes the parameters obtained at the modified electrodes with MPC. There is only one report on the MPC-based non-enzymatic electrochemical glucose biosensor [11]. It is seen that the sensors containing glucose oxidase have lower



**Table 2** The parameters of different electrodes modified with MPc for glucose detection

Electrode	Concentration range (mM)	Limit of detection	Sensitivity	Reference
NanoCoPc-glucose oxidase	0.02–18	5 $\mu\text{M}$	7.71 $\mu\text{A mM}^{-1} \text{cm}^{-2}$	[56]
CoPc-glucose oxidase	0.025–2	25 $\mu\text{M}$	1.170 $\mu\text{A mM}^{-1}$	[57]
Overoxidized polypyrrole nanofiber- CoPc tetrasulfonate	0.25–20	0.1 mM	5.695 $\mu\text{A mM}^{-1}$	[11]
glucose oxidase/CoPc nanorods on graphene	0.016–1.6	14.6 $\mu\text{M}$	–	[58]
NiPc	1.5–24	3 $\mu\text{M}$	0.08 $\mu\text{A mM}^{-1} \text{cm}^{-2}$	This work
NiPc-borophene nanocomposite		0.15 $\mu\text{M}$	10.31 $\mu\text{A mM}^{-1} \text{cm}^{-2}$	

detection limits than the non-enzymatic sensor containing polypyrrole nanobibers [56–58]. Although the detection limits of the sensors have been significantly improved, the use of enzymes has some disadvantages arising from their stabilities and the sensitivities to temperature. In this work, in addition to obtaining low detection limit values, NiPc-borophene nanocomposite sensor produced by adding borophene has a high sensitivity value.

## 4 Conclusions

The nanocomposite structure of NiPc with borophene, a highly conductive material has been shown to increase sensitivity and improve the detection limit of the sensor by overcoming the low conductivity problem, which is one of the disadvantages of phthalocyanines. For 1.5–24mM glucose concentration range, NiPc-based sensor has a sensitivity of 0.08  $\mu\text{AmM}^{-1} \text{cm}^{-2}$ , while the NiPc-borofen nanocomposite-based sensor has a much higher sensitivity, 10.31  $\mu\text{AmM}^{-1} \text{cm}^{-2}$  in 60 s cyclic voltammetry measurement. The detection limits of the NiPc and NiPc-borophene nanocomposite-based sensors are 3  $\mu\text{M}$  and 0.15  $\mu\text{M}$ , respectively. Therefore, it can be concluded that borophene is a good candidate to form nanocomposite structure with NiPc for non-enzymatic electrochemical detection of glucose. Moreover, due to its low cost, simple and environmentally friendly fabrication, portability and high sensitivity, this non-enzymatic sensor can offer an advantageous alternative to conventional sensors for glucose detection.

## Acknowledgements

The authors gratefully acknowledge the Scientific and Technological Research Council of Turkey (TUBITAK) for the financial support.

## Author contributions

All authors contributed to the study conception and design. Material preparation, data collection and analysis were performed by GB, İG, NT, SK and CT. The first draft of the manuscript was written by GB, NT contributed to conceptualization, methodology, reviewing, and editing of the manuscript. All authors commented on previous versions of the manuscript. All authors read and approved the final manuscript.

## Funding

This work was supported by TUBITAK. (Grant Number: 120N816)

## Data availability

The authors confirm that the data supporting the findings of this study are available within the article. Raw data that support the findings of this study are available from the corresponding author upon reasonable request.

## Declarations

**Conflict of interest** The authors declare no conflict of interest.

## References

1. J.D. Newman, A.P.F. Turner, *Biosens. Bioelectron.* **20**, 2435 (2005). <https://doi.org/10.1016/j.bios.2004.11.012>
2. A. Gaoa, X. Zhanga, X. Penga, H. Wua, L. Baib, W. Jina, G. Wua, R. Hanga, P.K. Chua, *Sens. Actuators B* **232**, 150 (2016). <https://doi.org/10.1016/j.snb.2016.03.122>
3. J.E. Shaw, R.A. Sicree, P.Z. Zimmet, *Diabetes Res. Clin. Pract.* **87**, 4 (2010). <https://doi.org/10.1016/j.diabres.2009.10.007>
4. Q. Yi, W. Huang, W. Yu, L. Li, X. Liu, *Electroanalysis* **20**, 206 (2008). <https://doi.org/10.1002/elan.200804282>
5. R. Wang, X. Liang, H. Liu, L. Cui, X. Zhang, C. Liu, *Microchim. Acta* **185**, 339 (2018). <https://doi.org/10.1007/s00604-018-2866-7>
6. K.K. Lee, P.Y. Loh, C.H. Sow, W.S. Chin, *Electrochem. Commun.* **20**, 128 (2012). <https://doi.org/10.1016/j.elecom.2012.04.012>
7. S. SoYoon, A. Ramadoss, B. Saravanakumar, S.J. Kim, *J. Electroanal. Chem.* **717–718**, 90 (2014). <https://doi.org/10.1016/j.jelechem.2014.01.012>
8. G. He, L. Tian, Y. Cai, S. Wu, Y. Su, H. Yan, W. Pu, J. Zhang, L. Li, *Nanoscale Res. Lett.* **13**, 3 (2018). <https://doi.org/10.1186/s11671-017-2406-0>
9. C. Tasaltın, T.A. Türkmen, N. Tasaltın, S. Karakus, *J. Mater. Sci.: Mater. Electron.* **32**, 10750 (2021). <https://doi.org/10.1007/s10854-021-05732-w>
10. N. Taşaltın, E. Aydın, S. Karakuş, A. Kilislioğlu, *Appl. Phys. A* **126**, 827 (2020). <https://doi.org/10.1007/s00339-020-03960-1>
11. L. Ozcan, Y. Sahin, H. Türk, *Biosens. Bioelectron.* **24**, 512 (2008). <https://doi.org/10.1016/j.bios.2008.05.004>
12. C. Li, Y. Su, X. Lv, H. Xia, H. Shi, X. Yang, J. Zhang, Y. Wang, *Biosens. Bioelectron.* **38**, 402 (2012). <https://doi.org/10.1016/j.bios.2012.04.049>
13. S. Mori, M. Nagata, Y. Nakahata, K. Yasuta, R. Goto, M. Kimura, M. Taya, *J. Am. Chem. Soc.* **132**, 4054 (2010). <https://doi.org/10.1021/ja9109677>
14. J.H. Zagal, S. Griveau, J.F. Silva, T. Nyokong, F. Bedioui, *Coord. Chem. Rev.* **254**, 2755 (2010). <https://doi.org/10.1016/j.ccr.2010.05.001>
15. P. Vasudevan, N. Phougat, A.K. Shukla, *Appl. Organomet. Chem.* **10**, 591 (1996)
16. M.M. Fadlallah, U. Eckern, A.H. Romero, U. Schwingenschlöggl, *New J. Phys.* **18**, 013003 (2016)
17. K.P. Madhuri, N.S. John, *Bull. Mater. Sci.* **41**, 118 (2018). <https://doi.org/10.1007/s12034-018-1636-9>
18. C.W. Foster, J.Pillay, J.P. Metters, C.E. Banks, *Sensors* **14**(11), 21905 (2014). <https://doi.org/10.3390/s141121905>
19. C.D. Kuhnline, M.G. Gangel, M.K. Hulvey, R.S. Martin, *Analyst* **131**(2), 202 (2006). <https://doi.org/10.1039/B511153F>
20. W.J.R. Santos, A.L. Sousa, R.C.S. Luz, F.S. Damos, L.T. Kubota, A. A.Tanaka, S. M.C.N.Tanaka, *Talanta* **70**, 588 (2006). <https://doi.org/10.1016/j.talanta.2006.01.023>
21. L.S. Vilakazi, T. Nyokong, *J. Electroanal. Chem.* **512**, 56 (2001). [https://doi.org/10.1016/S0022-0728\(01\)00583-6](https://doi.org/10.1016/S0022-0728(01)00583-6)
22. B.O. Agboola, S.L. Vilakazi, K.I. Ozoemena, *J. Solid State Electrochem.* **13**, 1367 (2009). <https://doi.org/10.1007/s10008-008-0691-3>
23. C.A. Caro, F. Bedioui, M.A. Páez, G.I. Cárdenas-Jiron, J.H. Zagal, *J. Electrochem. Soc.* **151**, E32 (2004). <https://doi.org/10.1149/1.1631822>
24. M.S. Liao, S. Scheiner, *J. Chem. Phys.* **114**, 9780 (2001). <https://doi.org/10.1063/1.1367374>
25. A.T. Chidembo, K.I. Ozoemena, B.O. Agboola, V. Gupta, G.G. Wildgoose, R.G. Compton, *Energy Environ. Sci.* **3**, 228 (2010). <https://doi.org/10.1039/B915920G>
26. L. Cui, T. Pu, Y. Liu, X. He, *Electrochim. Acta* **88**, 559 (2013). <https://doi.org/10.1016/j.electacta.2012.10.127>
27. H. Al-Sagur, S. Komathi, M.A. Khan, A.G. Gurek, A. Hassan, *Biosens. Bioelectron.* **92**, 638 (2017). <https://doi.org/10.1016/j.bios.2016.10.038>
28. S. Chaiyo, E. Mehmeti, W. Siangproh, T.L. Hoang, H.P. Nguyen, O. Chailapakul, K. Kalcher, *Biosens. Bioelectron.* **102**, 113 (2018). <https://doi.org/10.1016/j.bios.2017.11.015>
29. K.R. Mounesh, R. Venugopal, Fasiulla, *Anal. Chem. Lett.* **10**, 2 (2020). <https://doi.org/10.1080/22297928.2020.1760132>
30. S. Guo, S. Dong, *J. Mater. Chem.* **21**(46), 18503 (2011). <https://doi.org/10.1039/C1JM13228H>
31. D. Li, R.B. Kaner, *Science* **320**, 1170 (2008). doi:<https://doi.org/10.1126/science.1158180>
32. Z. Zhang, Y. Yang, G. Gao, B.I. Yakobson, *Angew. Chem. Int. Ed.* **127**, 13214 (2015). <https://doi.org/10.1002/anie.201505425>
33. Z. Zhang, S.N. Shirodkar, Y. Yang, B.I. Yakobson, *Angew. Chem. Int. Ed.* **129**, 15623 (2017). <https://doi.org/10.1002/anie.201705459>
34. L. Liu, Z. Zhang, X. Liu, X. Xuan, B.I. Yakobson, M.C. Hersam, W. Guo, *Nano Lett.* **20**(2), 1315 (2020). <https://doi.org/10.1021/acs.nanolett.9b04798>
35. Z. Zhang, A.J. Mannix, X. Liu, Z. Hu, N.P. Guisinger, M.C. Hersam, B.I. Yakobson, Near-equilibrium growth from borophene edges on silver. *Sci. Adv.* **5**, eaax0246 (2019). DOI:<https://doi.org/10.1126/sciadv.aax0246>
36. Z. Zhang, Y. Yang, E.S. Penev, B.I. Yakobson, *Adv. Funct. Mater.* **27**(9), 605059 (2017). <https://doi.org/10.1002/adfm.201605059>

37. Z. Zhuhua, E.S. Penev, B.I. Yakobson, Chem. Soc. Rev. **46**(22), 6746 (2017). <https://doi.org/10.1039/C7CS00261K>
38. L. Liu, Z. Zhang, X. Liu, X. Xuan, B.I. Yakobson, M.C. Hersam, W. Guo, Nano Lett. **20**, 1315 (2020). <https://doi.org/10.1021/acs.nanolett.9b04798>
39. I. Gürol, V. Ahsena, Ö. Bekaroğlu, J. Chem. Soc. Dalton Trans. **4**, 497 (1994). <https://doi.org/10.1039/DT9940000497>
40. M. Ma, T. Zhe, Y. Ma, Z. Wang, Q. Chen, J. Wang, Talanta **180**, 133 (2018). DOI:<https://doi.org/10.1016/j.talanta.2017.12.052>
41. M. Ou, X. Wang, L. Yu, C. Liu, W. Tao, X. Ji, L. Mei, Adv. Sci. **8**, 2001801, 1 (2021). <https://doi.org/10.1002/advs.202001801>
42. S. Güngör, C. Taşaltın, İ Gürol, G. Baytemir, S. Karakuş, N. Taşaltın, Appl. Phys. A **128**, 89 (2022). <https://doi.org/10.1007/s00339-021-05228-8>
43. R. Ridhi, S. Singh, G.S. S.Saini, S.K. Tripathi, J. Phys. Chem. Solids **115**, 119 (2018). <https://doi.org/10.1016/j.jpcs.2017.10.046>
44. C. Sittig, M. Textor, N.D. Spencer, M. Wieland, P.H. Val-lotton, J. Mater. Sci.: Mater. Med. **10**, 35 (1999). <https://doi.org/10.1023/a:1008840026907>
45. A.S. Mahmoud, R.S. Farag, M.M. Elshfai, Egypt. J. Petroleum **29**, 9 (2020). <https://doi.org/10.1016/j.ejpe.2019.09.001>
46. F.S. Torre, J.R. Rosa, B.I. Kharisov, C.J. Lucio-Ortiz, Materials **6**, 10, 4324 (2013). doi:<https://doi.org/10.3390/ma6104324>
47. S. Keshipour, S. Mohammad-Alizadeh, Sci. Rep. **11**, 16148 (2021). <https://doi.org/10.1038/s41598-021-95382-z>
48. K.W. Iwao Matsuda, *2D Boron: Boraphene, Borophene, Boronene*, 1st edn. (Springer, Cham, 2021)
49. H.-S. Tsai, C.-H. Hsiao, Y.-P. Lin, C.-W. Chen, H. Ouyang, J.-H. Liang, Small **12**(38), 5251 (2016). <https://doi.org/10.1002/sml.201601915>
50. T.V. Basova, V.G. Kiselev, B.-E. Schuster, H. Peisert, T. Chassé, J. Raman Spectrosc. **40**, 2080 (2009). <https://doi.org/10.1002/jrs.2375>
51. H. Chand, A. Kumar, V. Krishnan, Adv. Mater. Interfaces **8**, 2100045 (2021). <https://doi.org/10.1002/admi.202100045>
52. L. Kong, K. Wu, L. Chen, Front. Phys. **13**, 138105 (2018). <https://doi.org/10.1007/s11467-018-0752-8>
53. L. Dengfeng, C. Ying, H. Jia, T. Qiqi, Z. Chengyong, D. Guangqian, Chin. Phys. B **27**, 036303 (2018). <https://doi.org/10.1088/1674-1056/27/3/036303>
54. Z.-Q. Wang, T.-Y. Lü, H.-Q. Wang, Y.P. Feng, J.-C. Zheng, Front. Phys. **14**(2), 23403 (2019). <https://doi.org/10.1007/s11467-019-0884-5>
55. M. Nacef, M.L. Chelaghmia, A.M. Affoune, M. Pontié, Electroanalysis **31**(1), 113 (2019). <https://doi.org/10.1002/elan.201800622>
56. K. Wang, J.-J. Xu, H.-Y. Chen, Biosens. Bioelectron. **20**, 1388 (2005). <https://doi.org/10.1016/j.bios.2004.06.006>
57. E. Crouch, D.C. Cowell, S. Hoskins, R.W. Pittson, J.P. Hart, Biosens. Bioelectron. **21**, 712 (2005). <https://doi.org/10.1016/j.bios.2005.01.003>
58. H. Wang, Y. Bu, W. Dai, K. Li, H. Wang, X. Zuo, Sens. Actuators B **216**, 298 (2015). <https://doi.org/10.1016/j.snb.2015.04.044>

**Publisher's Note** Springer Nature remains neutral with regard to jurisdictional claims in published maps and institutional affiliations.